

# Redshift Evolution of the Type Ia Supernova Population Stretch Distribution

N. Nicolas <sup>\*1</sup>, M. Rigault <sup>\*\*2</sup>, R. Graziani<sup>2</sup>, M. Briday<sup>1</sup>, Y. Copin<sup>1</sup>, and Y. Kim<sup>1</sup>

<sup>1</sup> Université de Lyon, F-69622, Lyon, France; Université de Lyon 1, Villeurbanne; CNRS/IN2P3, Institut de Physique des Deux Infinis, Lyon

<sup>2</sup> Université Clermont Auvergne, CNRS/IN2P3, Laboratoire de Physique de Clermont, F-63000 Clermont-Ferrand, France.

Received 2 November 1992 / Accepted 7 January 1993

## ABSTRACT

**Context.** **ABSTRACT NOT DONE YET.** Type Ia supernovae (SNe Ia) allow for the construction of the Hubble diagram, giving us information about the Universe’s expansion and its fundamental components, one of which is dark energy. But systematic uncertainties are now starting to be limiting in our ability to measure those parameters. In particular, the physics of SNe Ia is still mostly unknown, and is thought not to change in time/with the redshift.

**Aims.** In an attempt to reduce those uncertainties, we try to find an empirical law describing SNe Ia’s length of explosion (stretch) evolution with the redshift.

**Methods.** We started by getting a complete sample representing all of the stretch distribution that Nature can give us, before using LsSFR measurements, an age tracer which evolution with redshift is known, that has been shown to have a strong correlation with the stretch. We compare their AIC, an estimator of the relative quality of statistical models that includes the number of free parameters, to determine which ones describe best the data.

**Results.** Models with an evolution of the stretch with the redshift have a better AIC than the ones without.

**Conclusions.** We find that implementing these models allows us to fit the data better than models without stretch evolution.

**Key words.** Cosmology – Type Ia Supernova – Systematic uncertainties

## 1. Introduction

Type Ia supernovae (SNe Ia) are powerful cosmological distance indicators that have enabled the discovery of the acceleration of the Universe’s expansion (Riess et al. 1998; Perlmutter et al. 1999). They remain today a key cosmological probe to understand the properties of dark energy (DE) as it is the only tool able to precisely map the recent expansion rate  $z < 0.5$ , when DE is driving it (e.g. Scolnic et al. 2019). They also are key to directly measure the Hubble Constant ( $H_0$ ), provided one can calibrate their absolute magnitude (Riess et al. 2016; Freedman et al. 2019). Interestingly, the value of  $H_0$  derived when the SNe Ia are anchored on Cepheids (the SH0ES project Riess et al. 2009, 2016) is  $\sim 5\sigma$  higher than what is predicted by cosmic microwave background (CMB) data measured by Planck assuming the standard  $\Lambda$ CDM, or when the SN luminosity is anchored at intermediate redshift by the baryon acoustic oscillation (BAO) scale (Riess et al. 2019; Reid et al. 2019; Planck Collaboration et al. 2016; Feeney et al. 2019). While using the tip of the red giant branch technique in place of the Cepheids seem to favor an intermediate value of  $H_0$  (Freedman et al. 2019), time delay measurements from strong lensing seem to also favor high  $H_0$  values (Wong et al. 2019).

The  $H_0$  tension has received a lot of attention as it could be a sign of new fundamental physics. Yet, no simple solution is able to accommodate this  $H_0$  tension when accounting for all other probes (Knox & Millea 2019) and the current most promising scenario appears to be a burst of expansion at the matter-

radiation decoupling moment caused by a (fine tuned) early dark energy (Poulin et al. 2019).

Alternatively, systematic effects affecting one or several of the aforementioned analysis could also explain the tension. In Rigault et al. (2015) we suggested that SNe Ia from the Cepheid calibrator sample differs by construction from the Hubble flow as it strongly favors young stellar population environments where one could find Cepheids. This selection effect would impact the derivation of  $H_0$  if SNe Ia from young and older environments differ in average magnitudes.

For the last decades, numerous analysis have studied the relation between SNe Ia and host properties, finding first that the standardized SNe Ia magnitude significantly depends on the host stellar-mass, SNe Ia from high-mass host being brighter on average (e.g. Kelly et al. 2010; Sullivan et al. 2010; Childress et al. 2013; Betoule et al. 2014; Rigault et al. 2018). This mass-step correction is currently used in cosmological analyses (e.g. Betoule et al. 2014; Scolnic et al. 2018), including for deriving  $H_0$  (Riess et al. 2016, 2019). Yet, the underlying connection between the SN and the host remains unclear when using global properties such as the host stellar mass, which raises the question of the accuracy of the correction. More recently, studies have used the local SN environment to probe more direct connections between the SN and its environments (Rigault et al. 2013), showing that local age-tracers such as the local specific star formation rate or the local color are more strongly correlated with the standardized SN magnitude (Rigault et al. 2018; Roman et al. 2018), suggesting the age to be the driving parameter underlying the mass-step. If true, this would have a significant impact for cosmology because the redshift drift magnitude correction to

\* n.nicolas@ipnl.in2p3.fr, equal contribution

\*\* m.rigault@ipnl.in2p3.fr, equal contribution

apply might strongly vary (Rigault et al. 2013; Childress et al. 2014; Scolnic et al. 2018). Yet, the importance of local SN environmental study remains highly debated (e.g. Jones et al. 2015, 2019) and especially the impact it has on the derivation of  $H_0$  (Jones et al. (2015); Riess et al. (2016, 2018); Rose et al. (2019)).

In this paper, we take a step aside to probe the validity of our modeling of the SN population that we claim to be constituted of two age-populations (Rigault et al. 2013; Rigault et al. 2015, 2018): one old and one young, the former having on average lower lightcurve stretches and being brighter after standardization. We indeed use the correlation between the SN age probed with local specific star formation rate in Rigault et al. (2018) and the SN stretch to model the expected evolution of the underlying SN stretch distribution as a function of redshift. This modeling relies on three assumptions: (1) there are indeed 2 populations of SNe Ia; (2) the relative fraction of each of these populations as a function of redshift follows the age-modeling made in (Rigault et al. 2018) and (3) the underlying distribution of stretch for each age-sample can be modeled and do not significantly drift. This paper aims at testing this with data from the literature.

The concept of the SNe Ia age dichotomy arised when the SN Ia rate has first been studied. Mannucci et al. (2005); Scannapieco & Bildsten (2005); Sullivan et al. (2006); Aubourg et al. (2008) have shown that the relative SNe Ia rate in galaxies could only be explained if two populations existed, one young, following the host star formation activity, and one old following the host stellar mass (the so called “prompt and delayed” or “A+B” model). In Rigault et al. (2018) we used the specific star formation rate at the SN location (Local sSFR or LsSFR) to classify which are the prompts (those with a high LsSFR) and which are the delayed (those with low LsSFR). Furthermore, since the first SNe Ia host analysis, the SN stretch has been known to be strongly correlated with the SN host properties (Hamuy et al. 1996, 2000), which has been extensively confirmed since (e.g. Neill et al. 2009; Sullivan et al. 2010; Lampeitl et al. 2010; Kelly et al. 2010; Gupta et al. 2011; D’Andrea et al. 2011; Childress et al. 2013; Rigault et al. 2013; Pan et al. 2014). Following the “A+B” model and the connection between SN stretch and host properties, Howell et al. (2007) first discussed the potential redshift drift of the SN stretch distribution. In this paper we revisit this analysis with the most recent SNe Ia dataset..

We present in section 2 the sample we are using for this analysis, which is based on the Pantheon dataset (Scolnic et al. 2018). We discuss the importance of obtaining a “complete” sample, i.e. representative of the true underlying SNe Ia distribution, and how we build one from the Pantheon sample. We then present in section 3 our modeling of the distribution of stretch as a function of redshift based stretch distribution of young and old SNe Ia. Our results are presented in section 4 where we test if the SN stretch does evolve as a function of redshift and if the age model is in good agreement with this evolution. Consequence for cosmology of our results are briefly discussed in section 5 and we conclude in section 6.

## 2. A “complete” Sample

We base our analysis on the latest SNe Ia compilation: the Pantheon catalog from Scolnic et al. (2018). A naive approach to test the SN stretch redshift drift would be to simply compare the observed SN stretch distributions in a few bins of redshift. In practice, selection effects are affecting the observed SN stretch distributions. Indeed, because the observed SN Ia magnitude correlates with the lightcurve stretch (and color), the first SN Ia that a magnitude-limited survey will miss are the reddest and

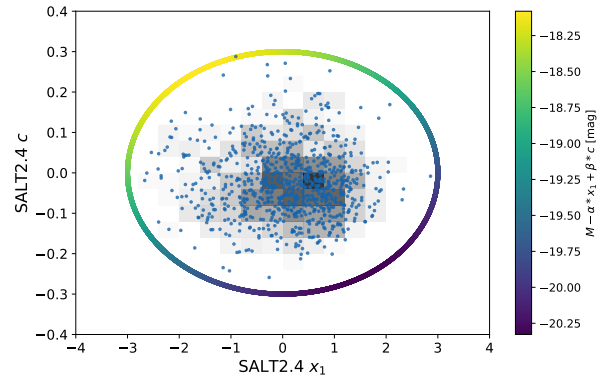


**Fig. 1.** SALT2.4 stretch and color lightcurve parameters of SNe Ia from the SDSS, PS1 and SNLS samples from the pantheon catalog. The individual SN data are shown as blue dots and a 2D histogram is shown in gray to highlight point density. The ellipse ( $x_1 = \pm 3$ ;  $c = \pm 0.3$ ) is displayed, colored by the corresponding standardized absolute magnitude using the  $\alpha$  and  $\beta$  coefficients from (Scolnic et al. 2018).

the lowest-stretch ones. Consequently, if selection effects are not accounted for, one might confuse true population drift with selection effects, and conversely.

Assuming sufficient (and random) spectroscopic follow-up for acquiring typing and host redshift, the selection effects of magnitude-limited survey should be negligible bellow a given redshift where even the faintest SNe Ia could be observed. In contrast, targeted surveys have highly complex selection functions and will be discarded from our analysis. Fortunately, modern SN cosmology samples such as the pantheon dataset are now dominated by magnitude limited surveys.

We present fig. 1 the lightcurve stretch and color distributions of SNe Ia from these surveys, namely: PanStarrs (PS1 Rest et al. 2014), the Sloan Digital Sky Survey (SDSS Frieman et al. 2008) and the SuperNovae Legacy Survey (SNLS Astier et al. 2006). An ellipse in the salt2.4 ( $x_1, c$ ) plan with semi-major axis  $x_1 = 3$  and semi-minor axis  $c = 0.3$  encapsulates the full distribution (Guy et al. 2007; Betoule et al. 2014); see also Bazin et al. (2011) and Campbell et al. (2013) for similar contours, the second using a more conservative  $c = 0.2$  cut. Assuming the SN absolute magnitude with  $x_1 = 0$  and  $c = 0$  is  $M_0 = -19.36$  (Kessler et al. 2009; Scolnic et al. 2014) we can derive the absolute standardized magnitude at maximum of light along the aforementioned ellipse given the standardization coefficient  $\alpha = 0.156$  and  $\beta = 3.14$  from Scolnic et al. (2018). The faintest SN Ia is that with  $x_1 = -1.66$  and  $c = 0.25$  and has an absolute standardized magnitude at peak in Bessel-b band of  $-18.31$  mag. Since one need to detect this object typically a week before and 10 days after peak to build a suitable lightcurve, the limiting standardized absolute magnitude effectively is approximately  $-18.00$  mag. Hence, given the  $5\sigma$  point source detection magnitude limit of a magnitude limited survey  $m_{lim}$ , one can derive the maximum redshift above which the faintest SNe Ia will be missed using the link between apparent magnitude, redshift and absolute magnitude given by:

$$m = \mu(z) + \underbrace{M_{min}^{t_0-10}}_{=-18.00 \text{ mag}}(x_1, c) < m_{lim} \quad (1)$$

SNLS typically acquires SNe Ia in the redshift range  $0.4 < z < 0.8$ . At these redshifts the rest-frame Bessel-B band roughly

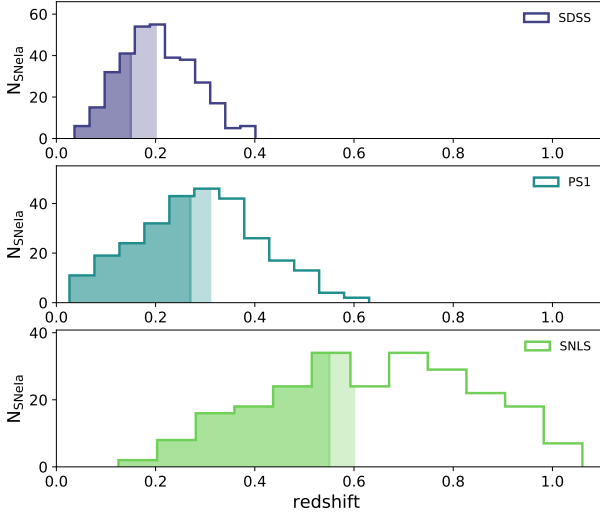


**Fig. 2.** From top to bottom: histogram of SN Ia redshifts for SDSS, PS1 and SNLS from the pantheon dataset, respectively. The colored part of the distribution shows which SNe Ia has been kept in our analysis for they are supposedly free from selection bias (see section 2). The full(light) color responds to the conservative(nominal) cut.

corresponds to the SNLS-*i* filter that has a 24.8 mag  $5\sigma$  depth<sup>1</sup>. This converts to a  $z_{lim} = 0.60$ , in perfect agreement with Neill et al. (2006), Perrett et al. (2010) and Bazin et al. (2011). Similarly, PS1 observes SNe Ia in the range  $0.2 < z < 0.4$ , their *g*-band  $5\sigma$  depth is 23.1 mag (Rest et al. 2014), which yields to  $z_{lim} = 0.30$  in agreement with, e.g., Figure 6 of Scolnic et al. (2018). This figure could also suggest a more conservative  $z_{lim}$  of 0.27; both will be considered as discussed below. In similar redshift range, SDSS has a limiting magnitude of 22.5 (Dilday et al. 2008; Sako et al. 2008), which would lead to a  $z_{lim} = 0.24$ . However, the SDSS surveys were more sensitive to limited spectroscopic resources. Kessler et al. (2009) pointed out that during year-1 of SDSS, SNe Ia with  $r - mag < 20.5$  were favored for spectroscopic follow up, corresponding to the redshift cut at 0.15. For the rest of the SDSS survey, additional spectroscopic resources were used, such that Kessler et al. (2009) and Dilday et al. (2008) show a relative completeness up to  $z_{lim} = 0.2$ . Following these analyses we will use  $z_{lim} = 0.2$  as the baseline SDSS redshift limit for the rest of this study. For the rest of the analysis, we will consider both cases, the aforementioned redshift limits as well as more conservative cuts for each of these surveys, namely  $z_{lim} = 0.15$  for SDSS,  $z_{lim} = 0.27$  for PS1 and  $z_{lim} = 0.55$  for SNLS, following Fig. 14 of Perrett et al. 2010.

The complete sample selection is summarized table 1 and the redshift distribution of these three surveys in are shown fig. 2. We see in this figure that the redshift limit we have selected roughly correspond to the peak of these histograms as expected.

In addition, we use the SNe Ia from the Nearby Supernova Factory (SNfactory Aldering 2004) published in Rigault et al. (2018) and that have been discovered from non-targeted searches (114 SNe Ia, see their section 3 and 4.2.2). As the searches were much deeper than the spectrophotometric follow-up made by SNfactory (SNf), SNe Ia within a redshift range of  $0.02 < z < 0.09$  (as in Rigault et al. 2018) should also be a random sampling of the underlying SN population. The SNf data is particularly useful for studying SN property drift as it enable us to have a large SN Ia sample at  $z < 0.1$ . The HST sample from

**Table 1.** Source surveys and number of SNe Ia used in our "complete" sample. Conservative cuts are indicated in brackets.

Survey	$z_{lim}$	$N_{SN}$
SNf	–	114
SDSS	0.20(0.15)	167(82)
PS1	0.30(0.27)	160(122)
SNLS	0.60(0.55)	102(78)
HST	–	26
Total	–	569(422)

Pantheon follows the same logic of having a search deeper than the follow-up and we therefore kept it entirely (?), see table 1.

### 3. Modeling the redshift drift

In Rigault et al. (2018) we presented a modeling of the evolution of the fraction of prompt and delayed SNe Ia as a function of redshift following former work on rates and delay time distributions (e.g., Mannucci et al. 2005; Scannapieco & Bildsten 2005; Sullivan et al. 2006; Aubourg et al. 2008; Childress et al. 2014; Maoz et al. 2014). In short, we assumed that the number of prompt SNe Ia follows the star formation activity in the Universe while the number of delayed SNe Ia follows the number of Gyr-old stars in the Universe, i.e. the stellar mass. Hence, if we denote  $\delta(z)$  (resp.  $\psi(z)$ ) the fraction of young (resp. old) SNe Ia in the Universe as a function of redshift, then their ratio  $\delta/\psi$  is expected to follow the evolution of the specific star formation rate which goes as  $(1+z)^{-2.8}$  until  $z \sim 2$  (e.g., Tasca et al. 2015). Hence since  $\delta(0.05) \sim \psi(0.05)$  (Rigault et al. 2013; Rigault et al. 2018; Wiseman et al. 2020), in agreement with rate expectations (Mannucci et al. 2006; Rodney et al. 2014), and  $\delta + \psi = 1$ , then we find in Rigault et al. (2018):

$$\delta(z) = \left( K^{-1} \times (1+z)^{-2.8} + 1 \right)^{-1} \text{ and} \quad (2)$$

$$\psi(z) = \left( K \times (1+z)^{+2.8} + 1 \right)^{-1} \quad (3)$$

where  $K = 0.87$ . This modelisation is comparable to the evolution predicted by Childress et al. (2014) based on SN rates in galaxies depending on their quenching time as a function of their stellar mass.

#### 3.1. Base underlying distribution

In Rigault et al. (2018) we presented the relation between SNe stretches and LsSFR measurements, which trace progenitor age, from the SNf sample, and is shown fig. 3. To model the evolution of the SN stretch as a function of redshift given our aforementioned model of the evolution of the fraction of young and old SNe Ia with redshift, we need to model the SN stretch distribution for each age subsample. Given the structure of the stretch–LsSFR scatter plot shown in fig. 3, we define our model as follows: for the young population the underlying stretch distribution is modeled as  $\mathcal{N}(\mu_1, \sigma_1^2)$ , i.e. a normal distribution centered on  $\mu_1$  with a  $\sigma_1$  width; the old population stretch distribution is modeled as  $a \times \mathcal{N}(\mu_1, \sigma_1^2) + (1-a) \times \mathcal{N}(\mu_2, \sigma_2^2)$ , i.e. a gaussian mixture where one mode is the same as the young population one. When combining our prediction of the evolution of young SNe Ia as a function of redshift eq. 2, and the stretch distribution

<sup>1</sup> CFHT final release website.

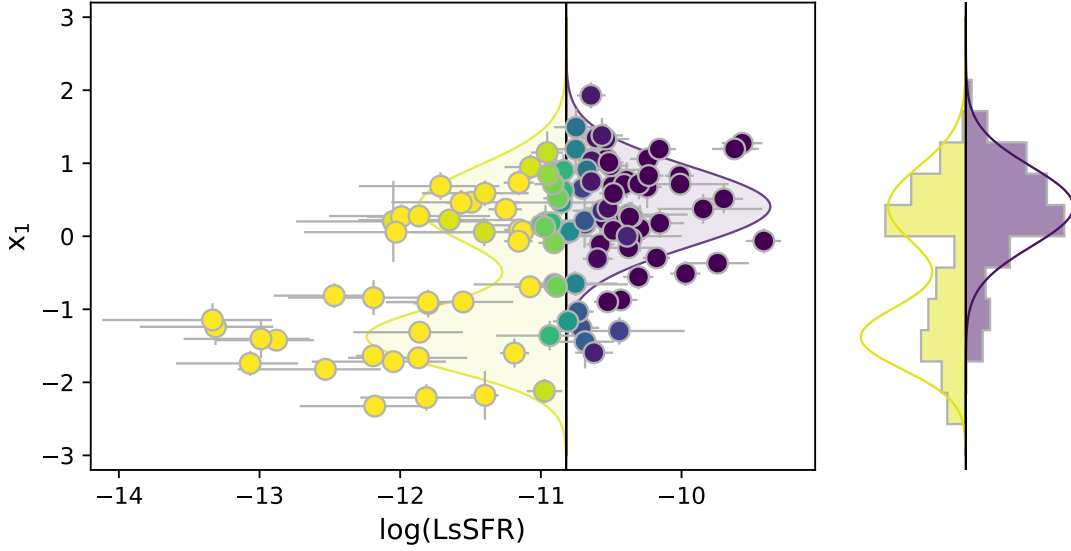


**Fig. 3.** *Main:* Salt2.4 lightcurve stretch ( $x_1$ ) as a function of the local specific star formation rate (LsSFR) for SNf data used in this analysis. The color corresponds to the probability for the SNe Ia to be above  $\log(\text{LsSFR} = -10.82)$ , which defines  $p(y)$ ; see Rigault et al. (2018). *Right:* histogram of  $p(y)$ -weighted marginalization of the SN stretch. On both panel, we illustrate the Base model fitted on the SNf data. The young and old population contributions are shown in purple and yellow, respectively.

of both young and SNe Ia, our model for the underlying distribution of stretch  $X_1(z)$  as a function of redshift is:

$$X_1(z) = \delta(z) \times \mathcal{N}(\mu_1, \sigma_1^2) + (1 - \delta(z)) \times [a \times \mathcal{N}(\mu_1, \sigma_1^2) + (1 - a) \times \mathcal{N}(\mu_2, \sigma_2^2)] \quad (4)$$

The estimation of the 5 free parameters ( $\theta \equiv \mu_1, \mu_2, \sigma_1, \sigma_2, a$ ) of the model is given by minimizing a pseudo- $\chi^2$   $\mathcal{L}$  such that:

$$\mathcal{L} = -2 \sum_i \ln(\mathcal{P}(x_1^i | \theta; dx_1^i, p(\text{young})^i)), \quad (5)$$

where  $i$  is the index of the SN Ia,  $x_1^i$ ,  $dx_1^i$  and  $p(\text{young})^i$  are the salt2.4 stretch, error of the salt2.4 stretch and the probability that the SN is young, respectively. Depending on the data available, there are two ways to fit these 5 free parameters.

### 3.1.1. Parameters estimation with LsSFR data

When using SNf data, we choose  $p(\text{young})$  to be their given  $p(y)$ , computed from their LsSFR data (see fig. 3). Thus, we would have  $\mathcal{P}$  from eq. 5 to be

$$\mathcal{P}(x_1^i | \theta; dx_1^i, p(\text{young})^i) = p(y)^i \times \mathcal{N}(\mu_1, \sqrt{\sigma_1^2 + dx_1^{i2}})(x_1^i) + (1 - p(y)^i) \times \left[ a \times \mathcal{N}(\mu_1, \sqrt{\sigma_1^2 + dx_1^{i2}})(x_1^i) + (1 - a) \times \mathcal{N}(\mu_2, \sqrt{\sigma_2^2 + dx_1^{i2}})(x_1^i) \right] \quad (6)$$

In practice, since " $a$ " is defined between 0 and 1, we fit for  $\alpha$  such that  $a = \arctan(\alpha)/\pi + 0.5$ , which results into asymmetric error on  $a$ . Results on fitting the SNf data with this model are shown table 2 and illustrated in fig. 3.

### 3.1.2. Without LsSFR data

Given eq. 4, we can extend the analysis to non-SNfactory sample by fitting the free parameters of the model ( $\theta \equiv \mu_1, \mu_2, \sigma_1, \sigma_2, a$ ) assuming the evolution of the fraction of young SNe Ia as a function of redshift given by  $\delta(z)$  and given, this time,  $x_1^i$ ,  $dx_1^i$  and  $z^i$ , the stretch, error on the stretch and redshift of any given SN  $i$ . In practice, it means that we are still minimizing for the same eq. 5, but replacing  $p(y)^i$  by  $\delta(z^i)$  eq. 6.

For the rest of the analysis, we will therefore fit for eq. 5 using  $p(y)^i$  – the probability for the SN  $i$  to be young – when available (i.e. for SNf dataset) and  $\delta(z^i)$  – the expected fraction of young SNe Ia at the SN redshift  $z^i$  – otherwise.

Results on fitting the all the 569(422) SNe Ia data (with conservative cuts) with this model are given table 2 and illustrated in fig. 4. We see in this figure that the measured mean SN Ia stretch per bin of redshift follow our redshift drift modeling. That is, when considering selection-bias free SN Ia samples, SNe Ia at higher redshift have on average larger stretch ( $0.34 \pm 0.10$  at  $z \sim 0.65$ ) than those at lower redshift ( $-0.17 \pm 0.10$  at  $z \sim 0.05$ ). This is indeed what is expected if old environments favor low SN stretch (Howell et al. 2007, e.g.) and if the fraction of old SNe Ia reduces as a function of redshift. See section 4 for a more quantitative discussion.

### 3.2. Other modelings

In section 3.1 we have modeled the underlying stretch distribution as a single gaussian for the young SNe Ia and a combination of two gaussians for the old SNe Ia population, i.e., the same as the young-population one plus another for the fast declining SNe Ia that seem to only exist in old populations. This is our "Base" model.

Howell et al. (2007) used a simpler modelisation: a single gaussian for each age sub-group. To test different modeling choices, we have implemented a suite of extra parametrisation that we also fit to the data following the procedure described section 3.1.2.



**Table 2.** Best fit values of the parameters for the Base stretch distribution model when applied to the SNf dataset only (114 SNe Ia), the nominal 569 SN Ia sample or the conservative one (422).

Sample	$\mu_1$	$\sigma_1$	$\mu_2$	$\sigma_2$	a
SNf	$0.41 \pm 0.08$	$0.55 \pm 0.06$	$-1.38 \pm 0.10$	$0.44 \pm 0.08$	$0.48^{+0.08}_{-0.08}$
All	$0.37 \pm 0.05$	$0.61 \pm 0.04$	$-1.22 \pm 0.16$	$0.56 \pm 0.10$	$0.51^{+0.09}_{-0.10}$
All(cons)	$0.38 \pm 0.05$	$0.60 \pm 0.04$	$-1.26 \pm 0.13$	$0.53 \pm 0.08$	$0.47^{+0.09}_{-0.08}$

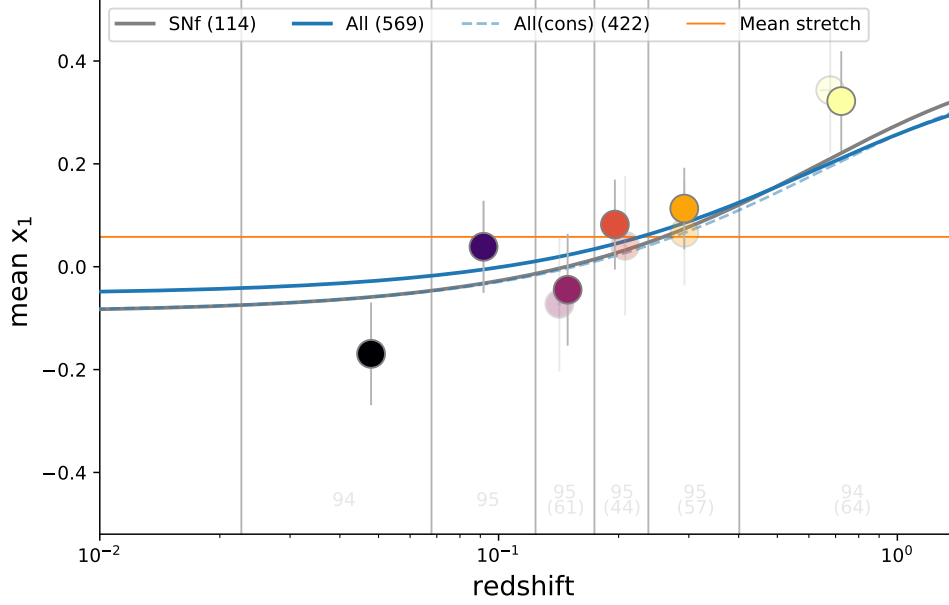


**Fig. 4.** Evolution of the mean SN salt2.4 stretch ( $x_1$ ) as a function of redshift. Markers show the mean stretch measured in redshift bins of equal sample size indicated in light gray at the bottom of each redshift bins. Full and light markers are used when considering the nominal or the conservative sample, respectively, and are colored by their mean redshift. The orange horizontal line represent the mean redshift of the nominal sample illustrating the expectation if the SN stretch distribution is not drifting. Best fits of our Base drifting model are shown as blue, dashed-blue and gray, when fitted on the nominal, the conservative or the SNf dataset, respectively; all are similar. The light-blue illustrate the amplitude of the error of the best fit model when considering the nominal dataset.

We thus consider a model “Howell+drift”, with one single gaussian per age group as in Howell et al. (2007). In addition, since we aim at probing the SN redshift drift, we are also fitting the “Base” model and this aforementioned extension by fixing the population drift parameter  $\delta(z)$  to a free parameter constant  $\delta(z) = f$ .

We are also considering alternative non-drifting models, and notably the one developed for the Beam with Bias Correction (BBC, Scolnic & Kessler 2016; Kessler & Scolnic 2017), currently used by all recent SN Cosmological analyses (e.g. Scolnic et al. 2018; Abbott et al. 2019; Riess et al. 2016, 2019) to account for Malmquist biases. The BBC formalism assumes sample-based (hence non-drifting) asymmetric Gaussian distributions ( $\mathcal{N}(\mu, \sigma^{-2}$  if  $x_1 < \mu$  else  $\sigma^+$ ). The idea behind the sample-based approach is twofold: (1) Malmquist biases are driven by survey properties and (2) because current surveys cover limited redshift ranges, doing so contains some potential redshift evolution information (Scolnic & Kessler 2016; Scolnic et al. 2018). See further discussion concerning the BBC modeling in section 5. For the sake of the comparison, we are also running Gaussian and asymmetric Gaussian non-drifting models.

The ability these models to explain the data is detailed in section 4.

## 4. Results

We applied each model on both the conservative and non-conservative samples (cf. section 2). Because the models presented section 3 have various degrees of freedom, we use the Akaike Information Criterion (AIC) (Burnham & Anderson 2004) to compare them. This estimator penalizes extra degrees of freedom to avoid over-fitting the data. It is defined as follow:

$$\text{AIC} = 2k - 2 \ln L \quad (7)$$

where  $k$  is the number of free parameters and  $-2 \ln L = \mathcal{L}$  is the pseudo- $\chi^2$  defined eq. (5). The reference model is the one with the smaller AIC and the probability for another model to be at least as representative of the data as this one is given by:

$$p(\text{other} \geq \text{ref}) = \exp(\Delta \text{AIC}/2) \quad (8)$$

Results are presented in table 3 and are illustrated fig. 5.

We find that underlying stretch distributions with no redshift drift are all excluded to describe the data as well as the best redshift models (i.e. Base and Base-( $\sigma_2$ )). In fact, the best non drifting model (Asymmetric) has  $2 \times 10^{-4}\%$  of chance to describe the data as well as Base-( $\sigma_2$ ), the best model. This is visible fig 4 where the mean stretches per bin of redshift of equal sample size suggest a redshift evolution following our Base model – fitted

**Table 3.** Comparison relative ability for a model to describe the data using AIC criterion. See the model definition section 3. The drift column indicates if the model contains the age-drifting model ( $\delta(z)$ ) or not (f, i.e. non-drifting). The BBC modeling is sample based which somewhat contains redshift dependency information.  $\mathcal{L}$  is the pseudo- $\chi^2$  defined eq. 5 and Proba is the probability that a model is at least as good as the reference model to describe the data. See also fig. 5.

Name	drift	Free param	$\mathcal{L}$	All SNe Ia (569)			All SNe Ia (conservative; 422)			
				AIC	$\Delta$ AIC	Proba	$\mathcal{L}$	AIC	$\Delta$ AIC	Proba
Base	$\delta(z)$	5	1456.7	1466.7	–	–	1079.5	1089.5	–	–
Howell	$\delta(z)$	4	1463.3	1471.3	-4.6	$1.0 \times 10^{-1}$	1088.2	1096.2	-6.7	$3.4 \times 10^{-2}$
Asymmetric	–	3	1485.2	1491.2	-24.5	$4.7 \times 10^{-6}$	1101.3	1107.3	-17.8	$1.4 \times 10^{-4}$
Howell	$f$	5	1484.2	1494.2	-27.5	$1.0 \times 10^{-6}$	1101.2	1111.2	-21.7	$1.9 \times 10^{-5}$
Base	$f$	6	1484.2	1496.2	-29.5	$3.9 \times 10^{-7}$	1101.2	1113.2	-23.7	$7.1 \times 10^{-6}$
BBC-modeling	per sample	3x5	1468.2	1498.2	-31.5	$1.5 \times 10^{-7}$	1083.6	1113.6	-24.1	$5.7 \times 10^{-6}$
Gaussian	–	2	1521.8	1525.8	-59.1	$1.5 \times 10^{-13}$	1142.6	1146.6	-57.1	$4.0 \times 10^{-13}$

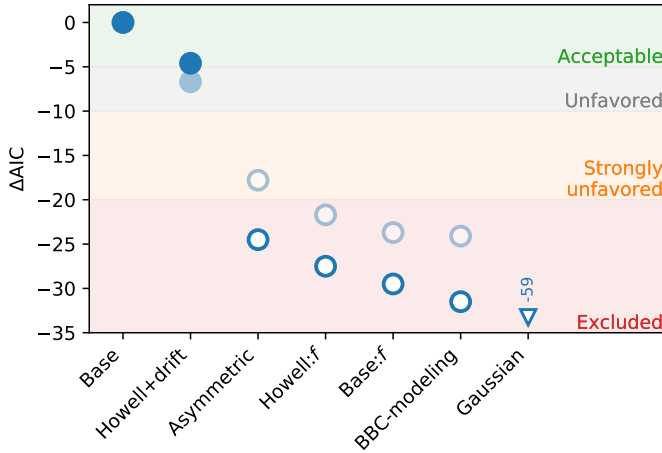


**Fig. 5.**  $\Delta$ AIC between the reference model and the other considered models (see also table 3). The full and open blue markers correspond to model with and without redshift drift, respectively. Light markers show the results when this analysis is done on the conservative sample. Color-bands illustrate the validity of the models, from Acceptable to Excluded, see inside text. All non-drifting models are excluded.

either on SNf, on the nominal 569 SNe Ia dataset or the conservative one – rather than having a constant mean value.

As just mentioned, the best model is Base-( $\sigma_2$ ) where both the low-stretch (mode 2 that only exists in old environments) and high-stretch (mode 1 that exists in all environments) normal distributions share the same width. It is marginally better than the Base model where both distributions have their own ( $\Delta$ AICc < 2). It is unclear which physical mechanism would translate into a simple distribution shift of mode 1 to a mode 2 that would only exist in old populations. Two distinct underlying distributions, as assumed by the Base model, seems more natural, yet, more data would be necessary to discriminate between these models. Similarly, letting the high-stretch distribution to vary between the young and the old population (Base+( $\mu_1^O, \sigma_1^O$ )) only marginally improves the fit ( $\Delta\mathcal{L} = 3.6$  in comparison to Base at a cost of 2 more degrees of freedom, making this mode less likely. This suggests that, indeed, the high-stretch mode (mode 1) exists in all kind of age-populations. We also remark that considering the stretch distribution of each age-population as independent normal distributions, as suggested by Howell et al. (2007), is 10 times less likely than our best model and is therefore unfavored.

Surprisingly, the BBC technique, which assumes an individual asymmetric distribution per sample (Scolnic & Kessler 2016; Kessler & Scolnic 2017), is one of the worst modelisation. While its pseudo- $\chi^2$   $\mathcal{L}$  is the best of all the non-drift model, but still  $\Delta\mathcal{L} = 11.3$  worse than our best model, it is penalized by requiring 15 free parameters, 3 per sample. Scolnic & Kessler (2016, section 2) and Scolnic et al. (2018, section 5.4) highlighted that, because current surveys span limited redshift ranges, the per sample approach somewhat account for unmodeled redshift drifts. We stress here that, as measure of modern surveys cover larger redshift ranges to reduce calibration systematic uncertainties, this is becoming less true, notably for PS1, DES and, soon, LSST. Already with the current surveys, the BBC sample-based technique is excluded to be an as good representation of the data as our best model ( $p = 4 \times 10^{-8}$ ). A more detailed discussion of the consequence of this results for cosmology follows in section 5

We report in table 4 the sample's  $\sigma^-$ ,  $\sigma^+$  and  $\mu^0$  that we find in close agreement with Scolnic & Kessler (2016) for SNLS and SDSS and with Scolnic et al. (2018) for PS1. This validates our somewhat simple construction of our selection-bias free sample, see section 2. If we were to use the Scolnic & Kessler (2016) and Scolnic et al. (2018) best fit values for SNLS, SDSS and PS1, respectively, the  $\Delta$ AICc between our Base drifting model and the BBC modeling would go from -32 to -47. Furthermore, fixing the Base model parameters to those derived using SNf data only (top row table. 2) and using the BBC parameters from the aforementioned literature for PS1, SDSS and SNLS, we find  $\Delta$ AICc = 31.7. Removing the SNf data reduces this difference to  $\Delta$ AICc = 5. Such a reduction is expected for two reasons. First, it removes the nearby SNe Ia, and thereby significantly reduces the redshift level arm to probe the impact of potential redshift drifts. Second, the SNf data are better at discriminating the individual stretch distributions by age since the probability for a SN to be young  $p(y^i)$  is known while other samples rely on  $\delta(z^i)$  which only is the fraction of young SNe Ia at the SN redshift, i.e. a proxy for  $p(y^i)$ . While in any case the Base-model is favored, the relative weight of a SNf sample highlight the importance of addition non-targeted nearby surveys such the Zwicky Transient Facility (ZTF, Bellm et al. 2019; Graham et al. 2019) to unambiguously confirm our result.

Considering or not the conservative sample has no effect on our conclusion as illustrated fig. 4 and presented table 3.

**Table 4.** Best fit parameters for our sample-based asymmetric modeling of the underlying stretch distribution.

Asymmetric	$\sigma^-$	$\sigma^+$	$\mu^0$
SNf	$1.34 \pm 0.13$	$0.41 \pm 0.10$	$0.68 \pm 0.15$
SDSS	$1.31 \pm 0.11$	$0.42 \pm 0.09$	$0.72 \pm 0.13$
PS1	$1.01 \pm 0.11$	$0.52 \pm 0.12$	$0.38 \pm 0.16$
SNLS	$1.41 \pm 0.13$	$0.15 \pm 0.13$	$1.22 \pm 0.15$
HST	$0.76 \pm 0.36$	$0.79 \pm 0.35$	$0.11 \pm 0.44$

## 5. Discussion

Our results strongly suggest that the underlying distribution of SN Ia stretch evolves as a function of redshift. Our redshift drift modeling presented section 3 is a much better representation of the pantheon data (see section 2) than any non-drifting models, including the sample-based BBC one.

To the best of our knowledge, the SN Ia stretch redshift drift has never been explicitly accounted for in cosmological analyses. Not doing so is a second order issue for SN cosmology as it only affects the way one does Malmquist bias correction. Indeed, as long as the Phillip’s relation standardization parameter  $\alpha$  is not redshift dependent (study behind the scope of this paper, but see e.g. Scolnic et al. 2018), if a sample is free from selection effects, the stretch-corrected SNe Ia magnitudes used for cosmology are blind to the underlying stretch distribution. However, since the first missed SNe Ia are the faintest, which are also those with the lowest stretch, once we include SNe Ia affected by selection effects we need to account for the fact that only the brightest SNe Ia exist in the low-stretch end of the sample after standardization. The modeling of the SN stretch then enters the analysis to understand which SNe Ia are missing given the selection functions to mimic a selection-bias free sample.

The state-of-the-art tool for doing so is the BBC described in Scolnic & Kessler (2016) and Kessler & Scolnic (2017), which is used in all recent SN Cosmological analyses (Jones et al. 2018; Scolnic et al. 2018; Brout et al. 2019; Abbott et al. 2019) including the direct measurement of  $H_0$  (Riess et al. 2016, 2019). As already discussed, it currently assumes an asymmetric stretch distribution per sample and we have shown in section 4 that this modeling is excluded to be as good description of the data than our age-based redshift drift modeling eq. 4.

We illustrate fig. 6 the prediction difference in the underlying stretch distribution between the BBC modeling and our Base drifting model for the PS1 sample. By definition, our model is bimodal and the relative amplitude of each mode depends on the fraction of old SNe Ia in the sample – the highest the fraction of old SNe Ia, the highest the amplitude of the low-stretch mode – and is therefore redshift dependent. As expected the two approaches strongly differ in modeling the negative part of the SN stretch distribution. The BBC asymmetric distribution goes in the middle of the bimodal distribution, largely over-estimating the number of SNe Ia at  $x_1 \sim -0.7$  and largely under-estimating it at  $x_1 \sim -1.7$  for typical PS1 SN redshifts. This means that the bias-correction of the individual SN stretch  $\bar{\delta}_{x_1}$  (Kessler & Scolnic 2017) and consequently the magnitude bias correction  $\mu_B$  is most likely inaccurate. However, given the complexity of the BBC analysis, a full study using our Base model given eq. 4 in place of the sample-based asymmetric modeling would be necessary to have an exact understanding of the effect this inaccurate modeling has on cosmology.

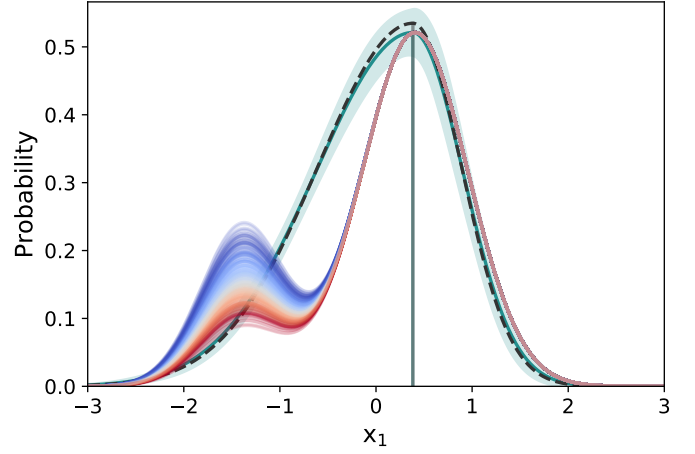


**Fig. 6.** Underlying SN salt2.4 stretch ( $x_1$ ) distributions for the PS1 sample. The Green line(band) shows our best fitted asymmetric Gaussian distribution (its error) mimicking the BBC approach. The dashed line shows that estimated by Scolnic et al. (2018). The blue to red curves display our Base drifting stretch model estimated at each PS SN redshift; bluer for lower redshifts.

Nonetheless, to have a rough estimation of the expected amplitude of the effect, we show fig. 7 the difference of mean stretch correction  $\alpha \times (\langle x_1 \rangle_{\text{BBC}} - \langle x_1 \rangle_{\text{Base}})$  as a function of redshift, using  $\alpha = 0.156$  from Scolnic et al. (2018). We see in this figure that the amplitude of the magnitude bias caused by an accurate modeling of the underlying stretch distribution is of the order of few tens of millimag, which is the typical scale exotic forms of dark energy could have on  $\mu(z)$ . In the era of modern cosmology where we aim at probing  $w_0$  at a sub-percent and  $w_a$  at a few percent (e.g., ?), it is therefore of paramount importance to further understand the exact modeling of the lightcurve parameters and especially their potential redshift drift; see also discussions about the impact of stretch and color distribution modeling for cosmology in Rubin et al. 2015 and Rubin & Hayden 2016.

## 6. Conclusion

We have presented a study of the drift of the underlying SNe Ia stretch distribution as a function of redshift. We used SNe Ia from magnitude-limited surveys from the pantheon data set (Scolnic et al. 2018, SDSS, PS1 and SNLS) as well as HST to which we added SNfactory data from Rigault et al. (2018) for the low-redshift bin. We only considered the supernovae that have been discovered in redshift ranges of each surveys where selection effect are negligible. This way the observed SNe Ia stretch are random sampling of the true underlying distribution. This corresponds the 569 SNe Ia (422 when considering more conservative cuts).

Following observations made in Rigault et al. (2018) we introduced a redshift drift modeling that depend on the expected fraction of young and old SNe Ia as a function of redshift, each age-population having its own underlying stretch distribution. We studied various suites of distribution as well as non-drifting modeling. We also closely studied the stretch distribution modeling made in current version of the BCC algorithm used for Malmquist bias correction by all recent Dark energy or Hubble constant cosmological analyses.

Our conclusion are the following:

1. Non-drifting models are excluded to be as good description of the data in comparison to our Base modeling. This model

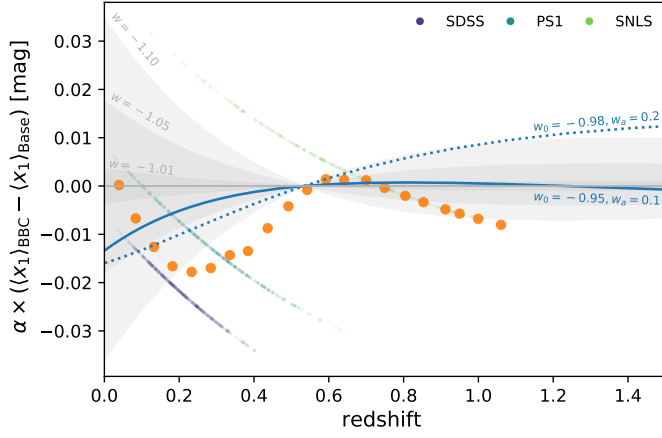


**Fig. 7.** Difference of mean stretch standardization (in mag) between the BBC algorithm used in Scolnic et al. (2018) and our Base drifting model. The blue markers represent the mean evolution in 30 regular redshift bins, while the small colored points show the SDSS, PS1 and SNLS samples. For comparison, we show in gray bands the expected magnitude difference between  $\Lambda$ CDM and  $w$ CDM cosmologies ( $w = -1 \pm 10, 5$  and  $1\%$ ) or, in orange, more exotic  $w_0, w_a$  CDM examples. This figure illustrates that the amplitude of the potential magnitude bias caused by inaccurate modeling of the underlying stretch distribution is comparable to the observational effect of exotic form of dark energy.

assumes that: (1) the young population has a unimodal Gaussian stretch distribution while the old population stretch one is bimodal, one mode been the young one; (2) the evolution of the relative fraction of young and old SNe Ia follows the prediction made in Rigault et al. (2018).

2. Given 1. we conclude that the SNe Ia is indeed drifting, as already suggested by (e.g. Howell et al. 2007).
3. The BBC approach, which assumes each survey to have its own asymmetric Gaussian distribution, is excluded to be an as good description of the data as our drifting model ( $p = 4 \times 10^{-8}$ ). Hence, the BBC sample-based approach does not accurately account for redshift drift as suggested by Scolnic & Kessler (2016) and Scolnic et al. (2018).
4. An inaccurate underlying stretch distribution modeling is estimated to bias the mean standardized SNe Ia on the order of a few percent, which is comparable in scale to the observational signature of exotic forms of dark energy.
5. We suggest to use the following stretch population modeling:

$$\Delta(x_1 | z) = \delta(z) \times \mathcal{N}(\mu_1, \sigma_1) + (1 - \delta(z)) \times [a \times \mathcal{N}(\mu_1, \sigma_1) + (1 - a) \times \mathcal{N}(\mu_2, \sigma_2)]$$

with:  $a = 0.50$ ,  $\mu_1 = 0.37$ ,  $\mu_2 = -1.22$ ,  $\sigma_1 = 0.61$ ,  $\sigma_2 = 0.56$ , see table 2 and using the age-population drift modelization  $\delta(z)$  defined in Rigault et al. (2018) with  $K = 0.87$ :

$$\delta(z) = \left( K^{-1} \times (1 + z)^{-2.8} + 1 \right)^{-1}$$

**Acknowledgements.** This project has received funding from the European Research Council (ERC) under the European Union’s Horizon 2020 research and innovation programme (grant agreement n 759194 - USNAC).

## References

Abbott, T. M. C., Abdalla, F. B., Alarcon, A., et al. 2018, Phys. Rev. D, 98, 043526  
 Abbott, T. M. C., Allam, S., Andersen, P., et al. 2019, ApJ, 872, L30  
 Aldering, G. 2004, APS April Meeting Abstracts 2004, V4.003

Astier, P., Guy, J., Regnault, N., et al. 2006, A&A, 447, 31  
 Ata, M., Kitaura, F.-S., Chuang, C.-H., et al. 2017, MNRAS, 467, 3993  
 Aubourg, É., Tojeiro, R., Jimenez, R., et al. 2008, A&A, 492, 631  
 Bazin, G., Ruhlmann-Kleider, V., Palanque-Delabrouille, N., et al. 2011, A&A, 534, A43  
 Bellm, E. C., Kulkarni, S. R., Graham, M. J., et al. 2019, PASP, 131, 018002  
 Betoule, M., Kessler, R., Guy, J., et al. 2014, A&A, 568, A22  
 Brout, D., Scolnic, D., Kessler, R., et al. 2019, ApJ, 874, 150  
 Burnham, K., Anderson, D., 2004, Sociological Methods & Research, 33, 2  
 Campbell, H., D’Andrea, C. B., Nichol, R. C., et al. 2013, ApJ, 763, 88  
 Chabanier, S., Millea, M., & Palanque-Delabrouille, N. 2019, MNRAS, 489, 2247  
 Childress, M., Aldering, G., Antilogus, P., et al. 2013, ApJ, 770, 108  
 Childress, M. J., Wolf, C., & Zahid, H. J. 2014, MNRAS, 445, 1898  
 Coles, P., & Jones, B. 1991, MNRAS, 248, 1  
 D’Andrea, C. B., Gupta, R. R., Sako, M., et al. 2011, ApJ, 743, 172  
 Dilday, B., Kessler, R., Frieman, J. A., et al. 2008, ApJ, 682, 262  
 Feeney, S. M., Peiris, H. V., Williamson, A. R., et al. 2019, Phys. Rev. Lett., 122, 061105  
 Freedman, W. L., Madore, B. F., Hatt, D., et al. 2019, ApJ, 882, 34  
 Frieman, J. A., Bassett, B., Becker, A., et al. 2008, AJ, 135, 338  
 Graham, M. J., Kulkarni, S. R., Bellm, E. C., et al. 2019, PASP, 131, 078001  
 Gupta, R. R., D’Andrea, C. B., Sako, M., et al. 2011, ApJ, 740, 92  
 Guy, J., Astier, P., Baumont, S., et al. 2007, A&A, 466, 11  
 Hamuy, M., Phillips, M. M., Suntzeff, N. B., et al. 1996, AJ, 112, 2391  
 Hamuy, M., Trager, S. C., Pinto, P. A., et al. 2000, AJ, 120, 1479  
 Howell, D. A., Sullivan, M., Conley, A., et al. 2007, ApJ, 667, L37  
 Jones, D. O., Riess, A. G., & Scolnic, D. M. 2015, ApJ, 812, 3  
 Jones, D. O., Riess, A. G., Scolnic, D. M., et al. 2018, ApJ, 867, 108  
 Jones, D. O., Scolnic, D. M., Riess, A. G., et al. 2018, ApJ, 857, 51  
 Jones, D. O., Scolnic, D. M., Foley, R. J., et al. 2019, ApJ, 881, 19  
 Kelly, P. L., Hicken, M., Burke, D. L., et al. 2010, ApJ, 715, 743  
 Kessler, R., Becker, A. C., Cinabro, D., et al. 2009, ApJS, 185, 32  
 Kessler, R., & Scolnic, D. 2017, ApJ, 836, 56  
 Knox, L., & Millea, M. 2019, arXiv e-prints, arXiv:1908.03663  
 Lampeitl, H., Smith, M., Nichol, R. C., et al. 2010, ApJ, 722, 566  
 Mannucci, F., Della Valle, M., Panagia, N., et al. 2005, A&A, 433, 807  
 Mannucci, F., Della Valle, M., & Panagia, N. 2006, MNRAS, 370, 773  
 Maoz, D., Mannucci, F., & Nelemans, G. 2014, ARA&A, 52, 107  
 Neill, J. D., Sullivan, M., Balam, D., et al. 2006, AJ, 132, 1126  
 Neill, J. D., Sullivan, M., Howell, D. A., et al. 2009, ApJ, 707, 1449  
 Pan, Y.-C., Sullivan, M., Maguire, K., et al. 2014, MNRAS, 438, 1391  
 Perlmutter, S., Aldering, G., Goldhaber, G., et al. 1999, ApJ, 517, 565  
 Perrett, K., Balam, D., Sullivan, M., et al. 2010, AJ, 140, 518  
 Planck Collaboration, Ade, P. A. R., Aghanim, N., et al. 2016, A&A, 594, A13  
 Poulin, V., Smith, T. L., Karwal, T., et al. 2019, Phys. Rev. Lett., 122, 221301  
 Planck Collaboration, Aghanim, N., Akrami, Y., et al. 2018, arXiv e-prints, arXiv:1807.06209  
 Reid, M. J., Pesce, D. W., & Riess, A. G. 2019, arXiv e-prints, arXiv:1908.05625  
 Rest, A., Scolnic, D., Foley, R. J., et al. 2014, ApJ, 795, 44  
 Riess, A. G., Filippenko, A. V., Challis, P., et al. 1998, AJ, 116, 1009  
 Riess, A. G., Macri, L., Casertano, S., et al. 2009, ApJ, 699, 539  
 Riess, A. G., Macri, L. M., Hoffmann, S. L., et al. 2016, ApJ, 826, 56  
 Riess, A. G., Casertano, S., Yuan, W., et al. 2018, ApJ, 861, 126  
 Riess, A. G., Casertano, S., Yuan, W., et al. 2019, ApJ, 876, 85  
 Rigault, M., Copin, Y., Aldering, G., et al. 2013, A&A, 560, A66  
 Rigault, M., Aldering, G., Kowalski, M., et al. 2015, ApJ, 802, 20  
 Rigault, M., Brinnel, V., Aldering, G., et al. 2018, arXiv:1806.03849  
 Rodney, S. A., Riess, A. G., Strolger, L.-G., et al. 2014, AJ, 148, 13  
 Roman, M., Hardin, D., Betoule, M., et al. 2018, A&A, 615, A68  
 Rose, B. M., Garnavich, P. M., & Berg, M. A. 2019, ApJ, 874, 32  
 Rubin, D., Aldering, G., Barbary, K., et al. 2015, ApJ, 813, 137  
 Rubin, D., & Hayden, B. 2016, ApJ, 833, L30  
 Sako, M., Bassett, B., Becker, A., et al. 2008, AJ, 135, 348  
 Scannapieco, E., & Bildsten, L. 2005, ApJ, 629, L85  
 Scolnic, D., Rest, A., Riess, A., et al. 2014, ApJ, 795, 45  
 Scolnic, D., & Kessler, R. 2016, ApJ, 822, L35  
 Scolnic, D. M., Jones, D. O., Rest, A., et al. 2018a, ApJ, 859, 101  
 Scolnic, D. M., Lochner, M., Gris, P., et al. 2018, arXiv e-prints, arXiv:1812.00516  
 Scolnic, D., Perlmutter, S., Aldering, G., et al. 2019, Astro2020: Decadal Survey on Astronomy and Astrophysics, 2020, 270  
 Sullivan, M., Le Borgne, D., Pritchet, C. J., et al. 2006, ApJ, 648, 868  
 Sullivan, M., Conley, A., Howell, D. A., et al. 2010, MNRAS, 406, 782  
 Tasca, L. A. M., Le Fèvre, O., Hathi, N. P., et al. 2015, A&A, 581, A54  
 Wiseman, P., Smith, M., Childress, M., et al. 2020, arXiv e-prints, arXiv:2001.02640  
 Wong, K. C., Suyu, S. H., Chen, G. C.-F., et al. 2019, arXiv e-prints, arXiv:1907.04869  
 Z